Heavy quarkonium dynamics at next-to-leading order in the binding energy over temperature

Michael Strickland
Kent State University
Kent, OH USA

N. Brambilla, M.-A. Escobedo, A. Islam, MS, A. Tiwari, A. Vairo, and P. Vander Griend, 2205.10289, to appear in JHEP

XQCD 2022, Trondheim, Norway
July 29, 2022

KENT STATE UNIVERSITY
U.S. DEPARTMENT OF ENERGY
TUM Global
Ohio Supercomputer Center
An OH·TECH Consortium Member

Bottomonium Suppression

- In a high temperature quark-gluon plasma we expect **weaker color binding** (Debye screening + asymptotic freedom)

  E. V. Shuryak, Phys. Rept. 61, 71–158 (1980)
  T. Matsui, and H. Satz, Phys. Lett. B178, 416 (1986)
  F. Karsch, M. T. Mehr, and H. Satz, Z. Phys. C37, 617 (1988)

- Also, high energy plasma particles which slam into the bound states cause them to have shorter lifetimes → **larger spectral widths**

TUMQCD Collaboration, 1804.10600

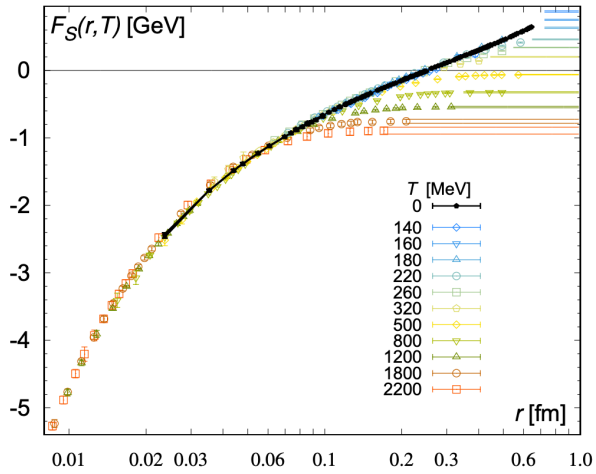

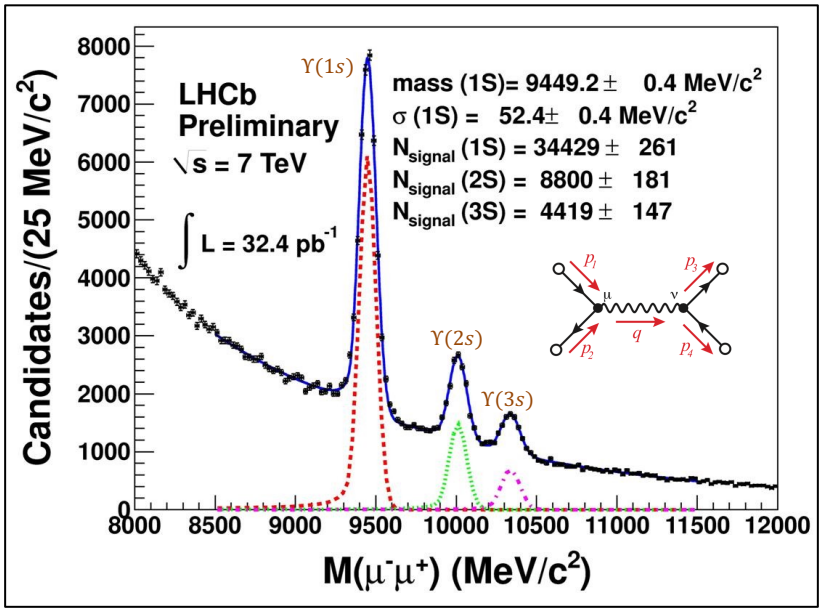

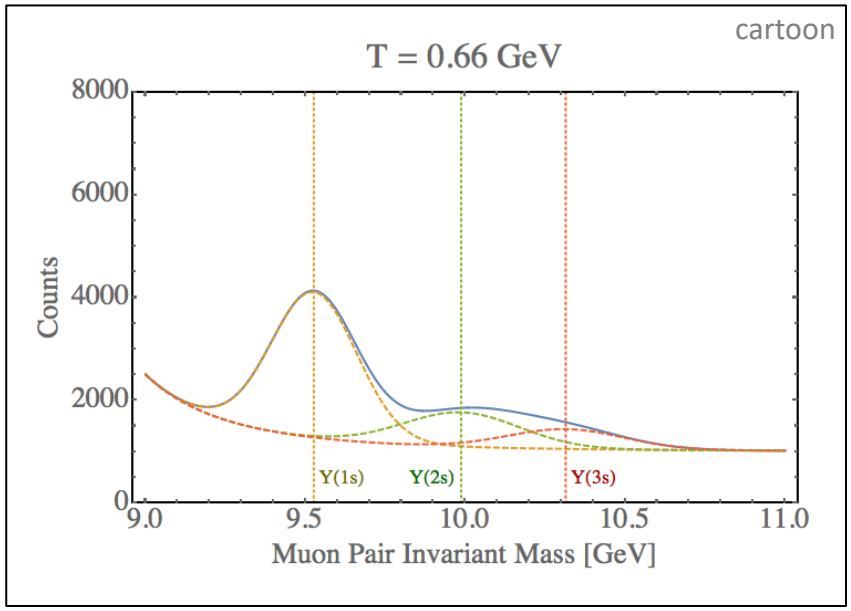

Experimental data – 5.02 TeV Dimuon Spectra

The **CMS, ALICE,** and **ATLAS** experiments have measured bottomonium production in both pp and Pb-Pb collisions at 5.02 TeV. Here I show CMS results.

pp

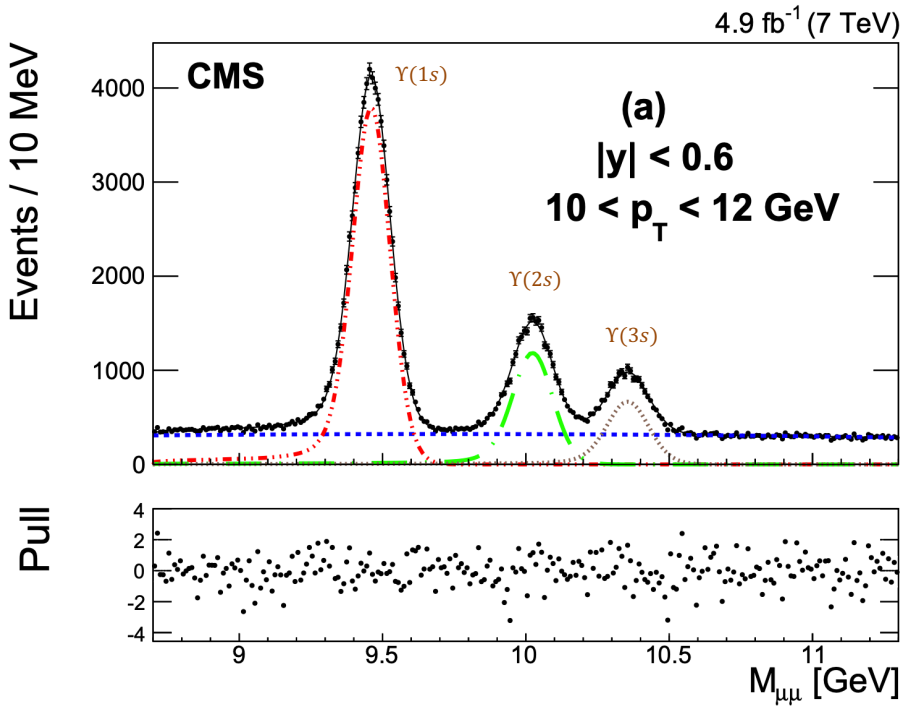

PbPb

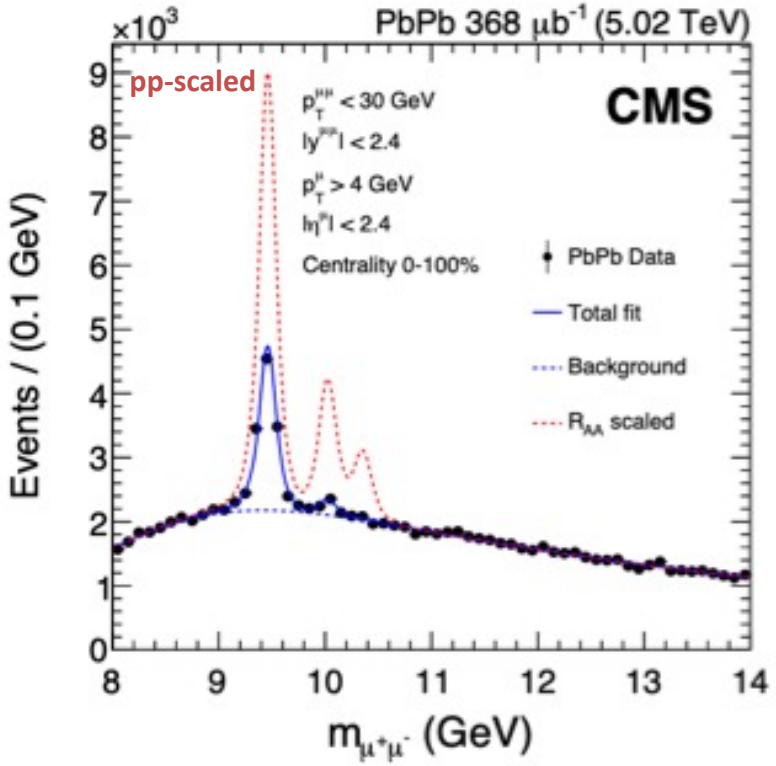

Why focus on bottomonia?

- Can trust heavy quark effective theory more.
- Cold nuclear matter (CNM) effects in AA decrease with increasing quark mass.
- The masses of bottomonia (m ~ 10 GeV) are much higher than the temperature generated in HICs (T < 1 GeV) → bottomonia production dominated by initial hard scatterings.

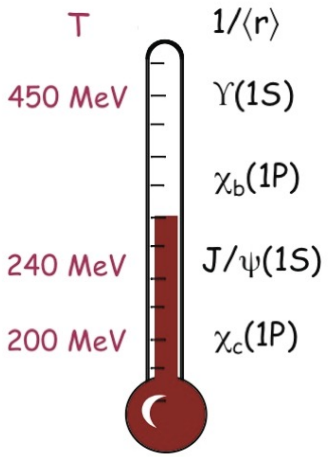

A. Mocsy, P. Petreczky, and MS, 1302.2180

- Since bottom quarks and anti-quarks are relatively rare in RHIC and LHC HICs, the probability for regeneration of bottomonia through statistical recombination is much smaller than for charm quarks. [see e.g. E. Emerick, X. Zhao, and R. Rapp, arXiv:1111.6537 and others]

Conceptual problem

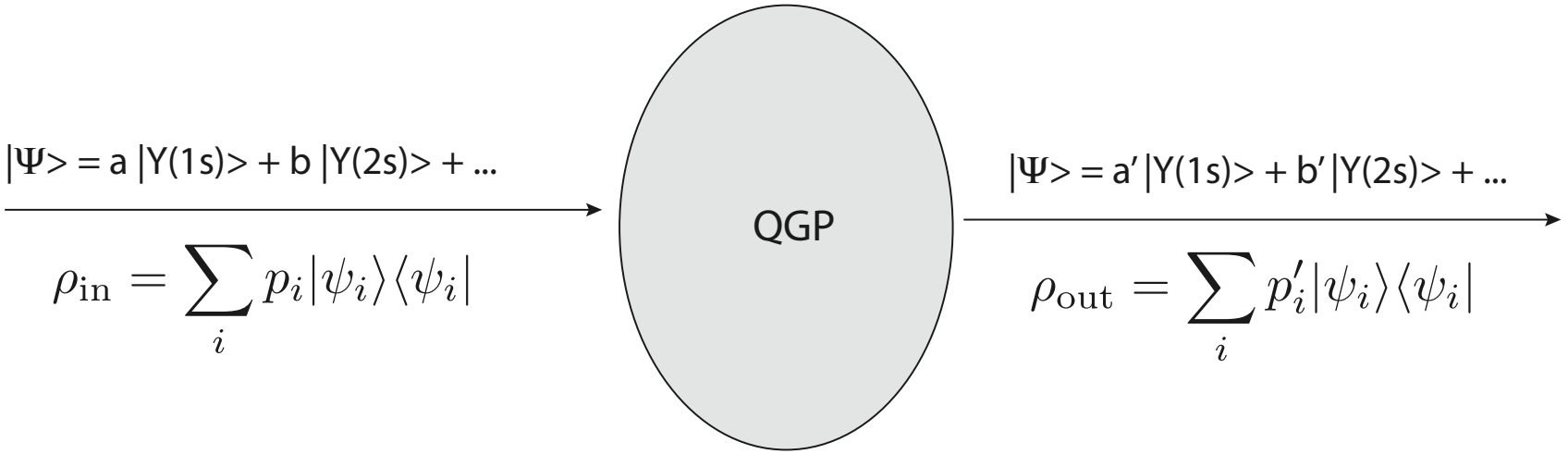

- Bottomonium states have a large binding energy (1S ~ 1 GeV) and are produced locally (hard processes) at early times in hard collisions (t < 1 fm/c).
- They then propagate through the plasma and interact with the medium.
- Bound states can break up and potentially re-form due to in-medium transitions induced by in-medium gluon absorption and emission.

Open quantum system (OQS) approach

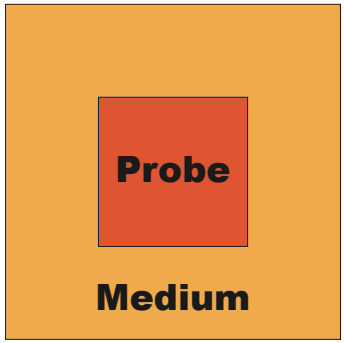

Probe = heavy-quarkonium state

Medium = light quarks and gluons that comprise the QGP

- Can treat heavy quarkonium states propagating through QGP using an open quantum system approach

$$H_{\rm tot} = H_{\rm probe} \otimes I_{\rm medium} + I_{\rm probe} \otimes H_{\rm medium} + H_{\rm int}$$

- Total density matrix

$$\rho_{\rm tot} = \sum_j p_j |\psi_j\rangle\langle\psi_j| \quad \longrightarrow \quad \frac{d}{dt}\rho_{\rm tot} = -i[H_{\rm tot}, \rho_{\rm tot}]$$

- Reduced density matrix (medium DOF integrated out)

$$\rho_{\rm probe} = {\rm Tr}_{\rm medium}[\rho_{\rm tot}] \quad \longrightarrow \quad \textbf{“Master equation”}$$

Bottomonium scales

- The mass scale is perturbative: $m_b \sim 5$ GeV
- The system is non-relativistic ($v \ll 1$), with $v_b \sim 0.1$.
- $\Delta_n E \sim mv^2$ and $\Delta_{\text{fs}} E \sim mv^4$

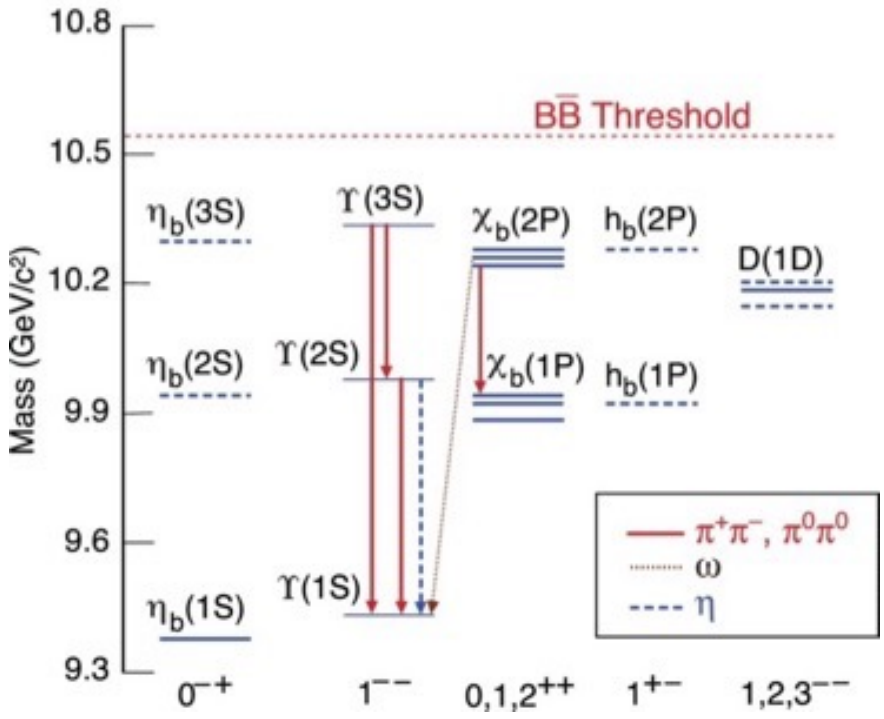

Results of a non-relativistic potential model

State	Name	Exp. [92]	Model	Rel. Err.
1^1S_0	$\eta_b(1S)$	9.398 GeV	9.398 GeV	0.001%
1^3S_1	$\Upsilon(1S)$	9.461 GeV	9.461 GeV	0.004%
1^3P_0	$\chi_{b0}(1P)$	9.859 GeV	9.869 GeV	0.21%
1^3P_1	$\chi_{b1}(1P)$	9.893 GeV		
1^3P_2	$\chi_{b2}(1P)$	9.912 GeV		
1^1P_1	$h_b(1P)$	9.899 GeV		
2^1S_0	$\eta_b(2S)$	9.999 GeV	9.977 GeV	0.22%
2^3S_1	$\Upsilon(2S)$	10.002 GeV	9.999 GeV	0.03%
2^3P_0	$\chi_{b0}(2P)$	10.232 GeV	10.246 GeV	0.05%
2^3P_1	$\chi_{b1}(2P)$	10.255 GeV		
2^3P_2	$\chi_{b2}(2P)$	10.269 GeV		
2^1P_1	$h_b(2P)$	-		
3^1S_0	$\eta_b(3S)$	-	10.344 GeV	-
3^3S_1	$\Upsilon(3S)$	10.355 GeV	10.358 GeV	0.03%

J. Alford and MS, 1309.3003

Non-Relativistic QCD (NRQCD)

Caswell and Lepage (1986), Bodwin, Braaten and Lepage (1994)

$$\mathcal{L}_{NRQCD} = \mathcal{L}_g + \mathcal{L}_q + \mathcal{L}_\psi + \mathcal{L}_\chi + \mathcal{L}_{\psi\chi}$$

$$\mathcal{L}_g = -\frac{1}{4}F^a_{\mu\nu}F^{\mu\nu a} + \frac{d_2}{m_Q^2}F^a_{\mu\nu}D^2F^{\mu\nu a} + d_g^3\frac{1}{m_Q^2}gf_{abc}F^a_{\mu\nu}F^{\mu b}_{\alpha}F^{\nu\alpha c}$$

$$\mathcal{L}_\psi = \psi^\dagger\left(iD_0 + c_2\frac{\mathrm{D}^2}{2m_Q} + c_4\frac{\mathrm{D}^4}{8m_Q^3} + c_F g\frac{\sigma\mathrm{B}}{2m_Q} + c_D g\frac{\mathrm{DE-ED}}{8m_Q^2} + ic_S g\frac{\sigma(\mathrm{D}\times\mathrm{E}-\mathrm{E}\times\mathrm{D})}{8m_Q^2}\right)\psi$$

$$\mathcal{L}_\chi = c.c\ of\ \mathcal{L}_\psi$$

$$\mathcal{L}_{\psi\chi} = \frac{f_1(^1S_0)}{m_Q^2}\psi^\dagger\chi\chi^\dagger\psi + \frac{f_1(^3S_1)}{m_Q^2}\psi^\dagger\sigma\chi\chi^\dagger\sigma\psi + \frac{f_8(^1S_0)}{m_Q^2}\psi^\dagger T^a\chi\chi^\dagger T^a\psi + \frac{f_8(^3S_1)}{m_Q^2}\psi^\dagger T^a\sigma\chi\chi^\dagger T^a\sigma\psi$$

- **Integrating out the scale m can be done perturbatively** and is not affected by the presence of the medium since $m \gg \Lambda_{QCD}, T$.
- **Hard gluons**, with energy and momentum of order m.
- **Soft gluons**, with energy and momentum of order mv.
- **Potential gluons**, with energy of order mv^2 and momentum of order mv.
- **Ultrasoft gluons**, with both energy and momentum of order mv^2

NRQCD → Potential NRQCD (pNRQCD)

Pineda and Soto, '97; Brambilla, Pineda, Soto, and Vairo '99, '00, '03

Degrees of freedom at the soft scale mv are integrated out

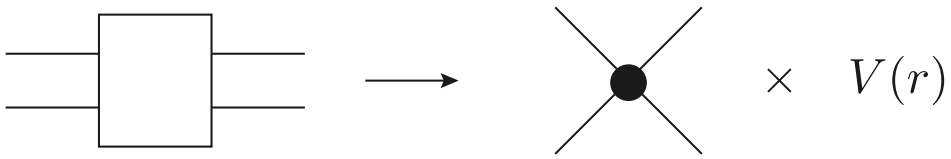

$$\times \quad V(r)$$

Power counting

$$r \sim \frac{1}{mv} \qquad t, R \sim \frac{1}{mv^2}, \frac{1}{\Lambda_{\rm QCD}}$$

Gauge fields are multiple expanded

$$A(r, R, t) = A(R, t) + \mathbf{r} \cdot \nabla A(R, t) + \dots$$

Non-analytic behavior in r → matching coefficients V

- Resulting degrees of freedom are singlet and octet states (see Lagrangian on next slide).
- Allows to obtain manifestly gauge-invariant results.
- Easier connection to lattice QCD.
- We can use this as a starting point.

NRQCD → Potential NRQCD (pNRQCD)

Pineda and Soto, '97; Brambilla, Pineda, Soto, and Vairo '99, '00, '03

$$\mathcal{L} = -\frac{1}{4}F^a_{\mu\nu}F^{\mu\nu,a} + \mathrm{Tr}\left\{ S^\dagger \left(i\partial_0 - \frac{\mathbf{p}^2}{m} - V_s \right) S + O^\dagger \left(i\partial_0 - \frac{\mathbf{p}^2}{m} - V_o \right) O \right\}$$

$$+V_A \,\mathrm{Tr}\left\{ O^\dagger\, \mathbf{r}\cdot g\mathbf{E}\, S + S^\dagger\, \mathbf{r}\cdot g\mathbf{E}\, O \right\} \rightarrow$$

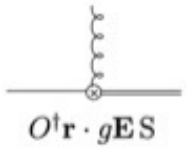

$$+\frac{V_B}{2}\,\mathrm{Tr}\left\{ O^\dagger\, \mathbf{r}\cdot g\mathbf{E}\, O + O^\dagger O\, \mathbf{r}\cdot g\mathbf{E} \right\} \rightarrow$$

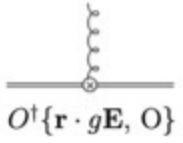

Singlet and octet potentials

$$V_s(r) = -C_F\frac{\alpha_s}{r}$$

$$V_o(r) = \frac{\alpha_s}{2N_c r}$$

- Based on this Lagrangian, we can perform first-principles calculations.
- Right figure shows diagrams contributing to singlet and octet self-energies.
- These enter into the calculation of Lindblad/collapse/jump operators.

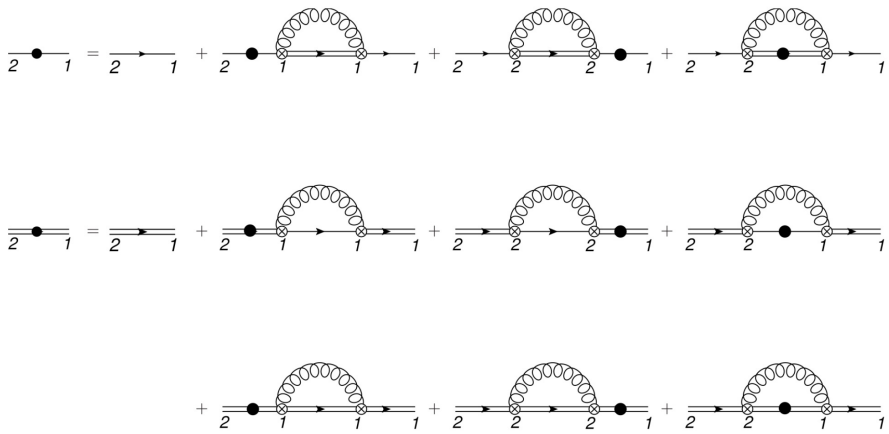

OQS + pNRQCD → Lindblad equation

- What are the relevant scales?
  - Temperature T
  - Bound state mass $m \gg T$
  - Bound state size $r \sim 1/mv \sim a_0$ (Bohr radius)
  - Debye mass m_D
  - Binding energy $E \sim mv^2$

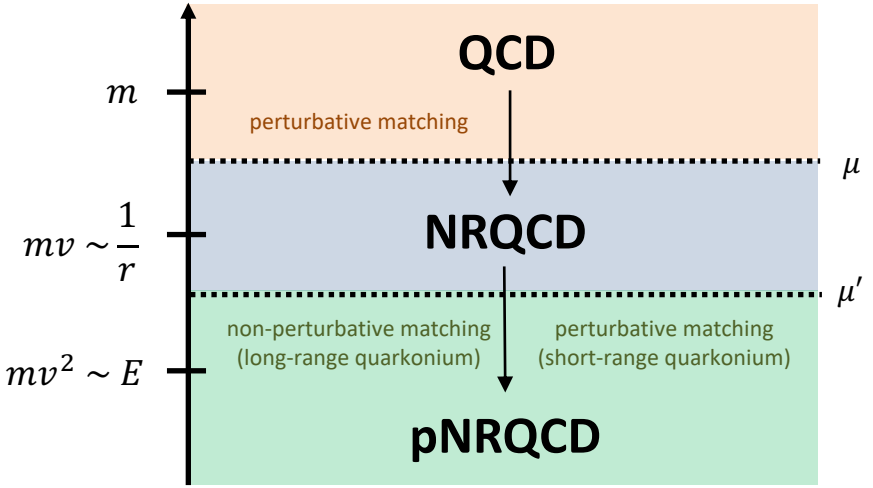

- Separation of time scales
  - Medium relaxation time scale $\langle \hat{O}_{\rm M}(t)\hat{O}_{\rm M}(0)\rangle \sim e^{-t/t_{\rm M}} \to \frac{1}{T}$
  - Intrinsic probe time scale $t_P \sim \frac{1}{\omega_i - \omega_j} \to \frac{1}{E}$
  - Probe relaxation time scale $\langle p(t)\rangle \sim e^{-t/t_{\rm rel}} \to \frac{1}{\text{self-energy}} \sim \frac{1}{\alpha_s a_0^2 \Lambda^3}$ $\quad \Lambda = T, E$

$1/r \gg T \sim m_D \gg E$

$t_{\rm rel}\,,\, t_{\rm P} \gg t_{\rm M}$

$$\frac{d\rho_{\rm probe}}{dt} = -i[H_{\rm probe}, \rho_{\rm probe}] + \sum_n \left(C_n\, \rho_{\rm probe}\, C_n^\dagger - \frac{1}{2}\{C_n^\dagger C_n, \rho_{\rm probe}\} \right)$$

N. Brambilla, M. A. Escobedo, J. Soto and A. Vairo, 1612.07248, 1711.04515

OQS + pNRQCD – Lindblad reorganization

$$\frac{d\rho_{\rm probe}}{dt} = -i[H_{\rm probe}, \rho_{\rm probe}] + \sum_n \left(C_n\, \rho_{\rm probe}\, C_n^\dagger - \frac{1}{2}\{C_n^\dagger C_n, \rho_{\rm probe}\} \right)$$

- $H_{\rm probe}$ is Hermitian (includes singlet and octet states)
- C_n are the **collapse (or jump) operators** (connect different internal states)
- Partial and **total decay width operators** are

$$\Gamma_n = C_n^\dagger C_n \qquad \Gamma = \sum_n \Gamma_n$$

- Can reorganize Lindblad equation by defining

$$H_{\rm eff} = H_{\rm probe} - \frac{i}{2}\Gamma$$

← **Non-Hermitian effective Hamiltonian**

$$\longrightarrow \quad \frac{d\rho_{\rm probe}}{dt} = -iH_{\rm eff}\rho_{\rm probe} + i\rho_{\rm probe}H_{\rm eff}^\dagger + \sum_n C_n\, \rho_{\rm probe}\, C_n^\dagger$$

LO OQS + pNRQCD Hamiltonian and collapse operators

N. Brambilla, M. A. Escobedo, J. Soto and A. Vairo, 1612.07248, 1711.04515

$$\frac{d\rho_{\rm probe}}{dt} = -iH_{\rm eff}\rho_{\rm probe} + i\rho_{\rm probe}H_{\rm eff}^\dagger + \sum_n C_n\,\rho_{\rm probe}\,C_n^\dagger$$

$$\rho = \begin{pmatrix} \rho_s & 0 \\ 0 & \rho_o \end{pmatrix}$$

$$H_{\rm probe} = \begin{pmatrix} h_s & 0 \\ 0 & h_o \end{pmatrix} + \frac{r^2}{2}\gamma \begin{pmatrix} 1 & 0 \\ 0 & \frac{N_c^2-2}{2(N_c^2-1)} \end{pmatrix}$$

mass shift

$$C_i^0 = \sqrt{\frac{\kappa}{N_c^2-1}}\, r^i \begin{pmatrix} 0 & 1 \\ \sqrt{N_c^2-1} & 0 \end{pmatrix},$$

$$C_i^1 = \sqrt{\frac{(N_c^2-4)\kappa}{2(N_c^2-1)}}\, r^i \begin{pmatrix} 0 & 0 \\ 0 & 1 \end{pmatrix}.$$

$$\Gamma = \kappa r^i \begin{pmatrix} 1 & 0 \\ 0 & \frac{N_c^2-2}{2(N_c^2-1)} \end{pmatrix} r^i$$

Total width → Im[V]

$$H_{\rm eff} = H_{\rm probe} - \frac{i}{2}\Gamma$$

Six collapse operators cover

- singlet → octet,
- octet → singlet
- octet → octet

$$\gamma \equiv \frac{g^2}{6\,N_c}\,{\rm Im}\int_{-\infty}^{+\infty} ds\,\langle T\,E^{a,i}(s,\mathbf{0})E^{a,i}(0,\mathbf{0})\rangle$$

$$\kappa \equiv \frac{g^2}{6\,N_c}\,{\rm Re}\int_{-\infty}^{+\infty} ds\,\langle T\,E^{a,i}(s,\mathbf{0})E^{a,i}(0,\mathbf{0})\rangle$$

LO OQS + pNRQCD Hamiltonian and collapse operators

N. Brambilla, M. A. Escobedo, J. Soto and A. Vairo, 1612.07248, 1711.04515

$$\frac{d\rho_{\rm probe}}{dt} = -iH_{\rm eff}\rho_{\rm probe} + i\rho_{\rm probe}H_{\rm eff}^{\dagger} + \sum_n C_n\,\rho_{\rm probe}\,C_n^{\dagger}$$

$$\rho = \begin{pmatrix} \rho_s & 0 \\ 0 & \rho_o \end{pmatrix}$$

$$C_i^0 = \sqrt{\frac{\kappa}{N_c^2-1}}\, r^i \begin{pmatrix} 0 & 1 \\ \sqrt{N_c^2-1} & 0 \end{pmatrix},$$

$$C_i^1 = \sqrt{\frac{(N_c^2-4)\kappa}{2(N_c^2-1)}}\, r^i \begin{pmatrix} 0 & 0 \\ 0 & 1 \end{pmatrix}.$$

Six collapse operators cover

- singlet → octet,
- octet → singlet
- octet → octet

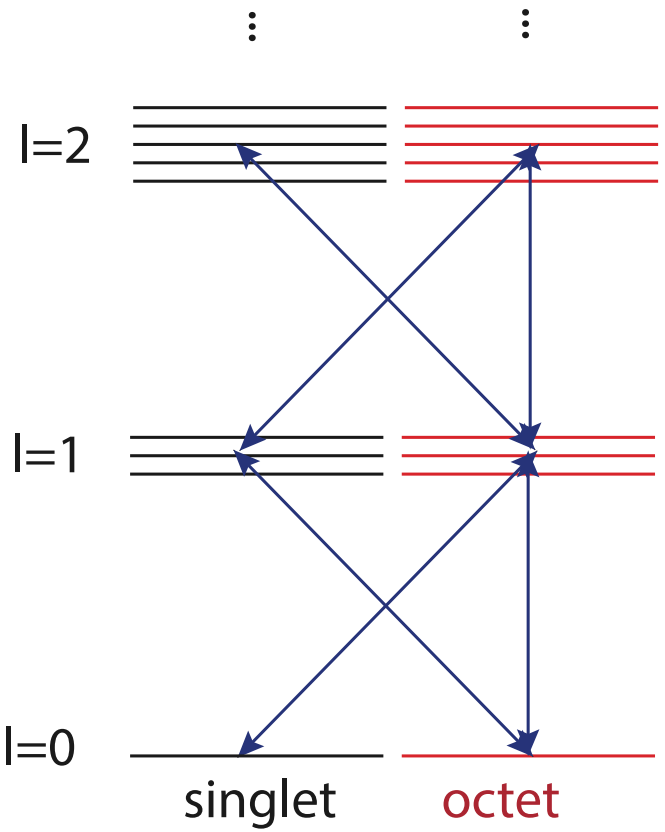

Going beyond leading order in E/T

N. Brambilla, M.-A. Escobedo, A. Islam, M.S., A. Tiwari, A. Vairo, and P. Vander Griend, 2205.10289

- Results on previous slides were obtained by truncating at leading order (LO) in E/T (binding energy over temperature). This was extended to NLO in the reference above.

- By decomposing states into radial and angular components, for an isotropic system we can rewrite the operators as acting only on the 1d effective wavefunction
  u(r,t) = r R(r,t).

- At NLO, there are six jump operators (shown on the right).

- Based on these, one can write down the singlet and octet non-Hermitian effective Hamiltonian (see ref above for details).

$$C^{\uparrow}_{s\to o} = r - \frac{N_c\alpha_s}{8T} + \frac{1}{2MT}\left(\frac{\partial}{\partial r} - \frac{l+1}{r}\right),$$
$$C^{\downarrow}_{s\to o} = r - \frac{N_c\alpha_s}{8T} + \frac{1}{2MT}\left(\frac{\partial}{\partial r} + \frac{l}{r}\right),$$
$$C^{\uparrow}_{o\to s} = r + \frac{N_c\alpha_s}{8T} + \frac{1}{2MT}\left(\frac{\partial}{\partial r} - \frac{l+1}{r}\right),$$
$$C^{\downarrow}_{o\to s} = r + \frac{N_c\alpha_s}{8T} + \frac{1}{2MT}\left(\frac{\partial}{\partial r} + \frac{l}{r}\right),$$
$$C^{\uparrow}_{o\to o} = r + \frac{1}{2MT}\left(\frac{\partial}{\partial r} - \frac{l+1}{r}\right),$$
$$C^{\downarrow}_{o\to o} = r + \frac{1}{2MT}\left(\frac{\partial}{\partial r} + \frac{l}{r}\right).$$

Full NLO effective Hamiltonian

N. Brambilla, M.-A. Escobedo, A. Islam, M.S., A. Tiwari, A. Vairo, and P. Vander Griend, 2205.10289

The effective Hamiltonian for singlet and octet evolution is defined by $H_{s,o}^{\rm eff} = h_{s,o} + {\rm Im}(\Sigma_{s,o}) - i\Gamma_{s,o}/2$ with $\Gamma_s = \sum_{i\in\{\uparrow,\downarrow\}} \Gamma^i_{s\to o}$ and $\Gamma_o = \sum_{i\in\{\uparrow,\downarrow\}} (\Gamma^i_{o\to s} + \Gamma^i_{o\to o})$. When expressed as operators acting on the reduced wave function, the singlet effective Hamiltonian $\overline{H}_s^{\rm eff}$ is given by

$$
{\rm Re}[\overline{H}_s^{\rm eff}] = \frac{\overline{\mathcal{D}}^2}{M} - \frac{C_f\,\alpha_{\rm s}}{r} + \frac{\hat{\gamma}T^3}{2} r^2 + \frac{\hat{\kappa}T^2}{4M}\{r, p_r\}\,, \tag{3.12}
$$

$$
{\rm Im}[\overline{H}_s^{\rm eff}] = -\frac{\hat{\kappa}T^3}{2}\left[\left(r - \frac{N_c\alpha_{\rm s}}{8T}\right)^2 - \frac{3}{2MT} + \frac{\overline{\mathcal{D}}^2}{(2MT)^2} + \frac{1}{2MT}\left(\frac{N_c\alpha_{\rm s}}{4T}\right)\frac{1}{r}\right], \tag{3.13}
$$

where $p_r = -i\partial_r$. Similarly, the octet effective Hamiltonian $\overline{H}_o^{\rm eff}$ is given by

$$
{\rm Re}[\overline{H}_o^{\rm eff}] = \frac{\overline{\mathcal{D}}^2}{M} + \frac{1}{2N_c}\frac{\alpha_{\rm s}}{r} + \frac{N_c^2-2}{2(N_c^2-1)}\left[\frac{\hat{\gamma}T^3}{2} r^2 + \frac{\hat{\kappa}T^2}{4M}\{r, p_r\}\right], \tag{3.14}
$$

$$
\begin{aligned}
{\rm Im}[\overline{H}_o^{\rm eff}] = &-\frac{\hat{\kappa}T^3}{2(N_c^2-1)}\left[\left(r + \frac{N_c\alpha_{\rm s}}{8T}\right)^2 - \frac{3}{2MT} + \frac{\overline{\mathcal{D}}^2}{(2MT)^2} - \frac{1}{2MT}\left(\frac{N_c\alpha_{\rm s}}{4T}\right)\frac{1}{r}\right] \\
&-\frac{\hat{\kappa}T^3}{4(N_c^2-1)}\left[r^2 - \frac{3}{2MT} + \frac{\overline{\mathcal{D}}^2}{(2MT)^2}\right],
\end{aligned} \tag{3.15}
$$

where $\hat{\kappa} = \kappa/T^3$ and $\hat{\gamma} = \gamma/T^3$.

$$
\overline{\mathcal{D}}^2 = -\frac{\partial^2}{\partial r^2} + \frac{l(l+1)}{r^2}
$$

Values of $\hat{\kappa}$ and $\hat{\gamma}$ used

- We used NLO fits to recent lattice measurements of the heavy quark transport coefficient $\hat{\kappa} \equiv \kappa/T^3$. Note that this is related to the heavy quark diffusion constant D.
  - N. Brambilla, V. Leino, P. Petreczky, and A. Vairo, 2007.10078

N. Brambilla, V. Leino, P. Petreczky, and A. Vairo, 2007.10078

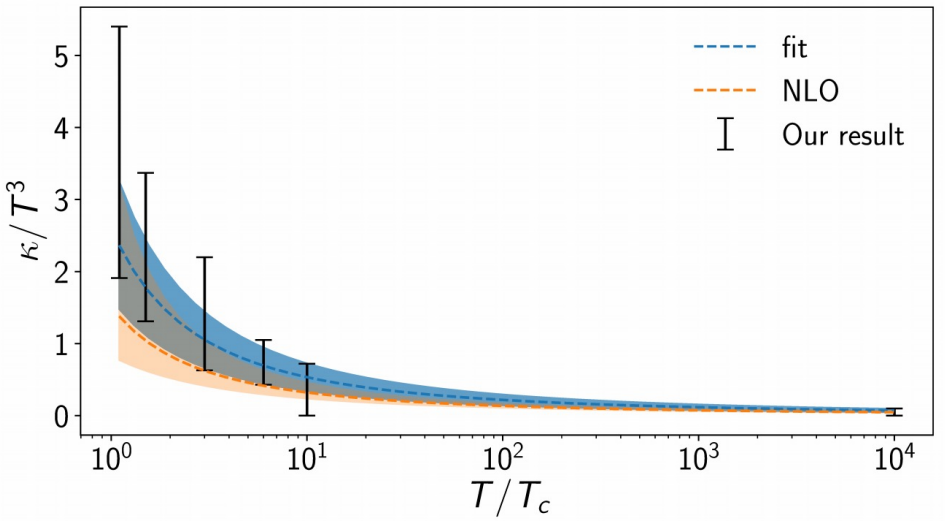

- The value of $\hat{\gamma} \equiv \gamma/T^3$ is less constrained, we vary it in the range -3.5 < $\hat{\gamma}$ < 0.
  - N. Brambilla, M. A. Escobedo, J. Soto and A. Vairo, 1612.07248.
  - N. Brambilla, M. A. Escobedo, J. Soto and A. Vairo, 1711.04515.
  - N. Brambilla, M. A. Escobedo, A. Vairo and P. Vander Griend, 1903.08063.

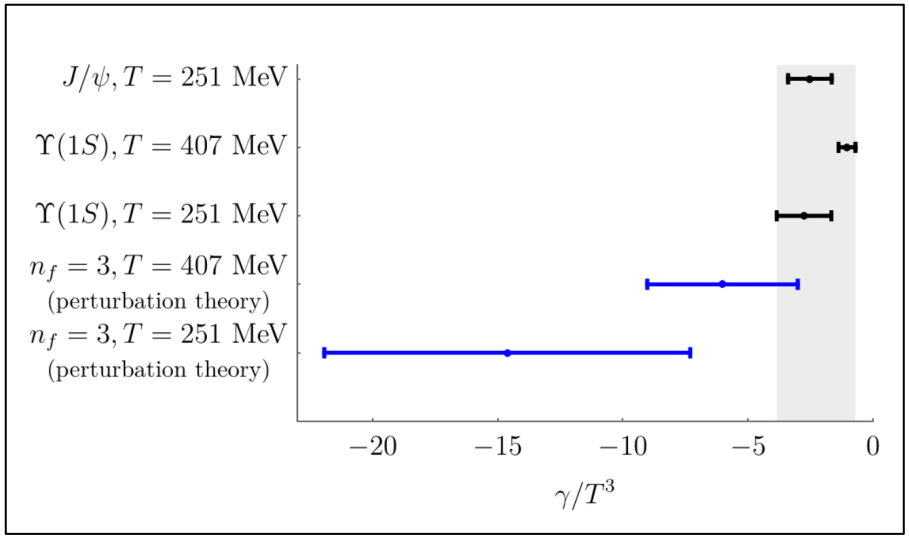

N. Brambilla, M. A. Escobedo, A. Vairo and P. Vander Griend, 1903.08063.

Computing survival probabilities with QTraj

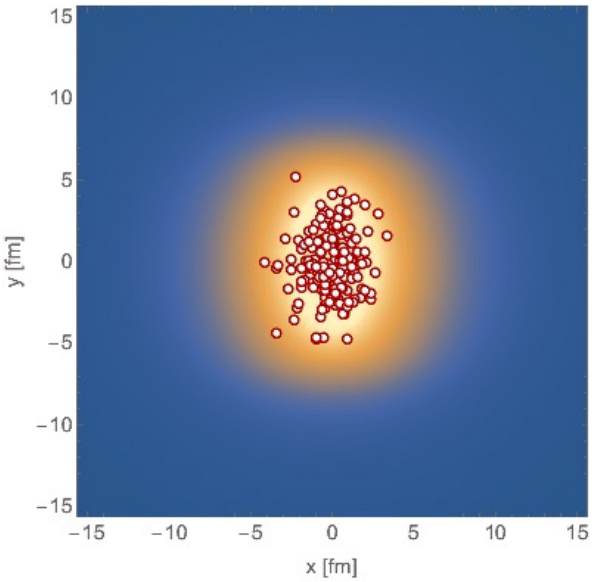

Survival probability

$$SP(n,l) = \frac{|\langle n,l|\psi(t_f)\rangle|^2}{|\langle n,l|\psi(t_0)\rangle|^2}$$

- Used $N = 4096$ points
- $L = 108\, a_0$
- $\Delta t = 2 \times 10^{-4}$ fm

- We sampled bottomonium production points and initial COM transverse momentum using **Monte-Carlo sampling** (physical trajectories).
- Temperature evolution provided **by 3+1D anisotropic hydrodynamics** (good description of identified soft hadron spectra and anisotropic flow, see backup slides for evidence).
- Along each physical trajectory, we solved the **real-time 3D Schrödinger equation with a complex potential and stochastically sampled jumps** → Lindblad equation.
- We then solved for the **survival probability** of S- and P-wave states (see box to the left).

Feed-down implementation

$$\vec{N}_{\text{observed}} = F\vec{N}_{\text{direct}}$$

$$F = \begin{pmatrix} 1 & 0.2645 & 0.0194 & 0.352 & 0.18 & 0.0657 & 0.0038 & 0.1153 & 0.077 \\ 0 & 1 & 0 & 0 & 0 & 0.106 & 0.0138 & 0.181 & 0.089 \\ 0 & 0 & 1 & 0 & 0 & 0 & 0 & 0 & 0 \\ 0 & 0 & 0 & 1 & 0 & 0 & 0 & 0.0091 & 0 \\ 0 & 0 & 0 & 0 & 1 & 0 & 0 & 0 & 0.0051 \\ 0 & 0 & 0 & 0 & 0 & 1 & 0 & 0 & 0 \\ 0 & 0 & 0 & 0 & 0 & 0 & 1 & 0 & 0 \\ 0 & 0 & 0 & 0 & 0 & 0 & 0 & 1 & 0 \\ 0 & 0 & 0 & 0 & 0 & 0 & 0 & 0 & 1 \end{pmatrix}$$

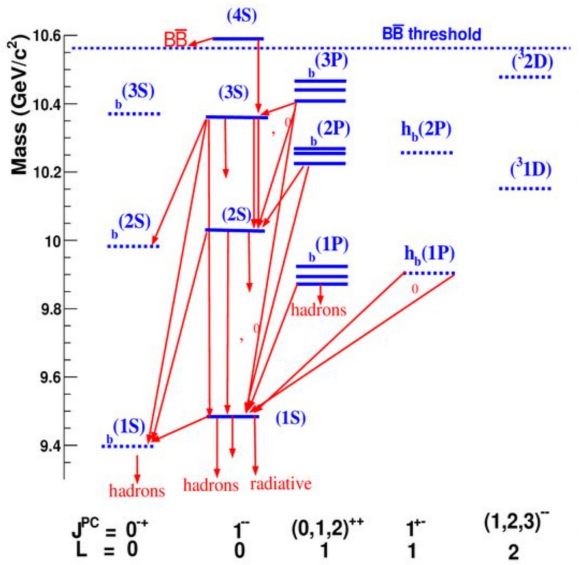

- N_{direct} corresponds to (N_{1S}, N_{2S}, N_{1P} x 3, N_{3S}, N_{2P} x 3, N_{2D})^T where, e.g., N_{1S} is the final number of Y(1S) states that can decay in the dilepton channel.
- N_{direct} can be obtained using $\langle N_{bin}(b) \rangle * \sigma_{direct} *$ (Survival probability)
- After feed down, we then normalize by the pp collision result scaled to AA → R_{AA}.

$$R^i_{AA}(c) = \frac{(F \cdot S(c) \cdot \vec{\sigma}_{\text{direct}})^i}{\sigma^i_{\text{exp}}}$$

NLO OQS + pNRQCD predictions for R_{AA} vs N_{part} at LHC

N. Brambilla, M.-A. Escobedo, A. Islam, M.S., A. Tiwari, A. Vairo, P. Vander Griend, 2205.10289

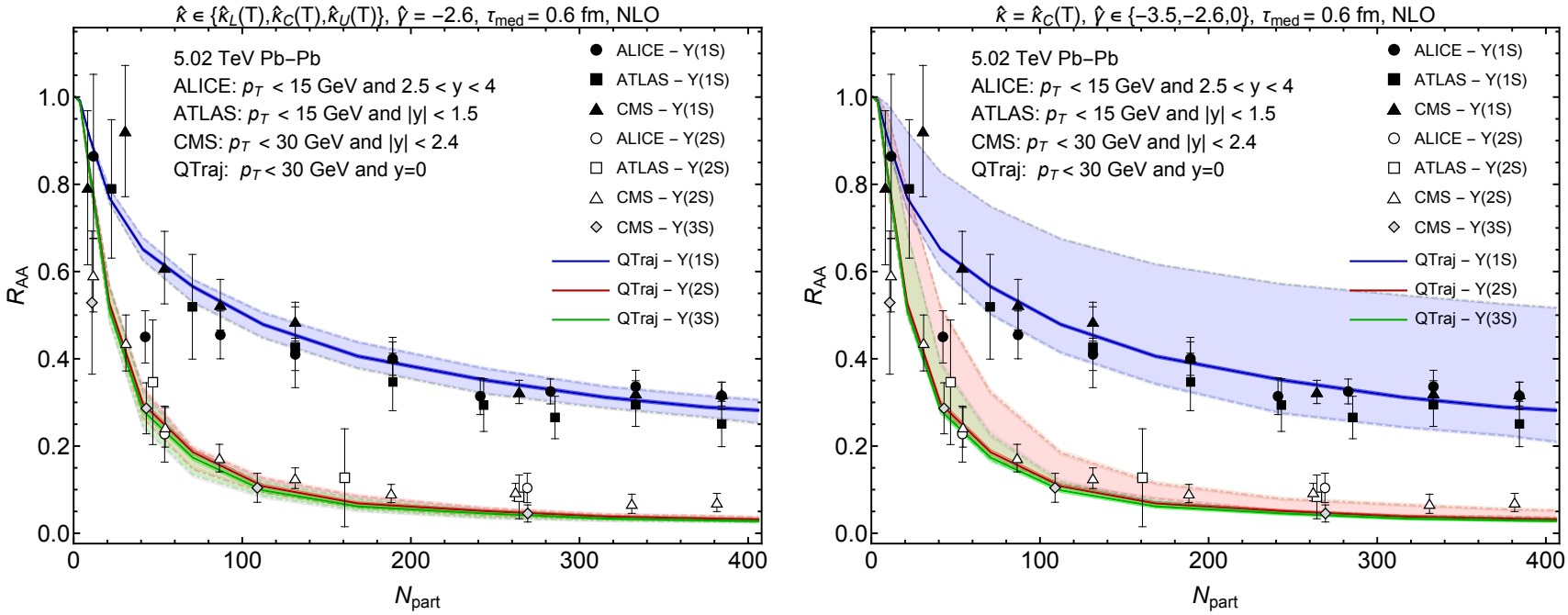

- **Left panel**: Result including feed down, when varying $\hat{\kappa}$ over the theoretical uncertainty.
- **Right panel**: Result including feed down, when varying $\hat{\gamma}$ over the theoretical uncertainty
- **Note:** The NLO results above ignore jumps (H_{eff} only). The effect of jumps is expected to be small based on prior studies, but requires lots of computer time (forthcoming).
- The statistical uncertainty associated with the average over physical trajectories is on the order of the line width.

NLO R_{AA} vs transverse momentum

N. Brambilla, M.-A. Escobedo, A. Islam, M.S., A. Tiwari, A. Vairo, P. Vander Griend, 2205.10289

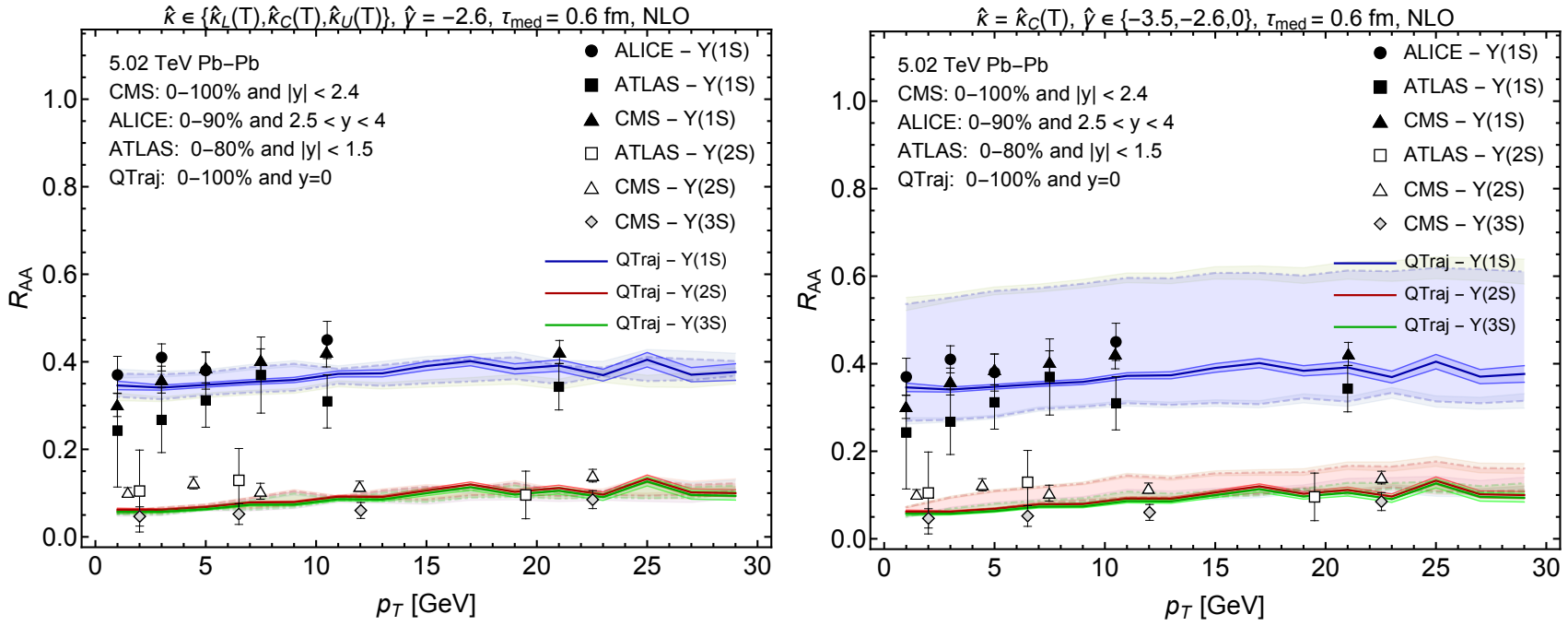

- QTraj predictions consistent with experimental observations.
- Very flat. Small decrease comes from longer time spent in the QGP as the velocity decreases.
- Once again, larger variation from uncertainty in $\hat{\gamma}$.

NLO OQS + pNRQCD predictions for R_{AA} vs N_{part} at LHC

N. Brambilla, M.-A. Escobedo, A. Islam, M.S., A. Tiwari, A. Vairo, P. Vander Griend, 2205.10289

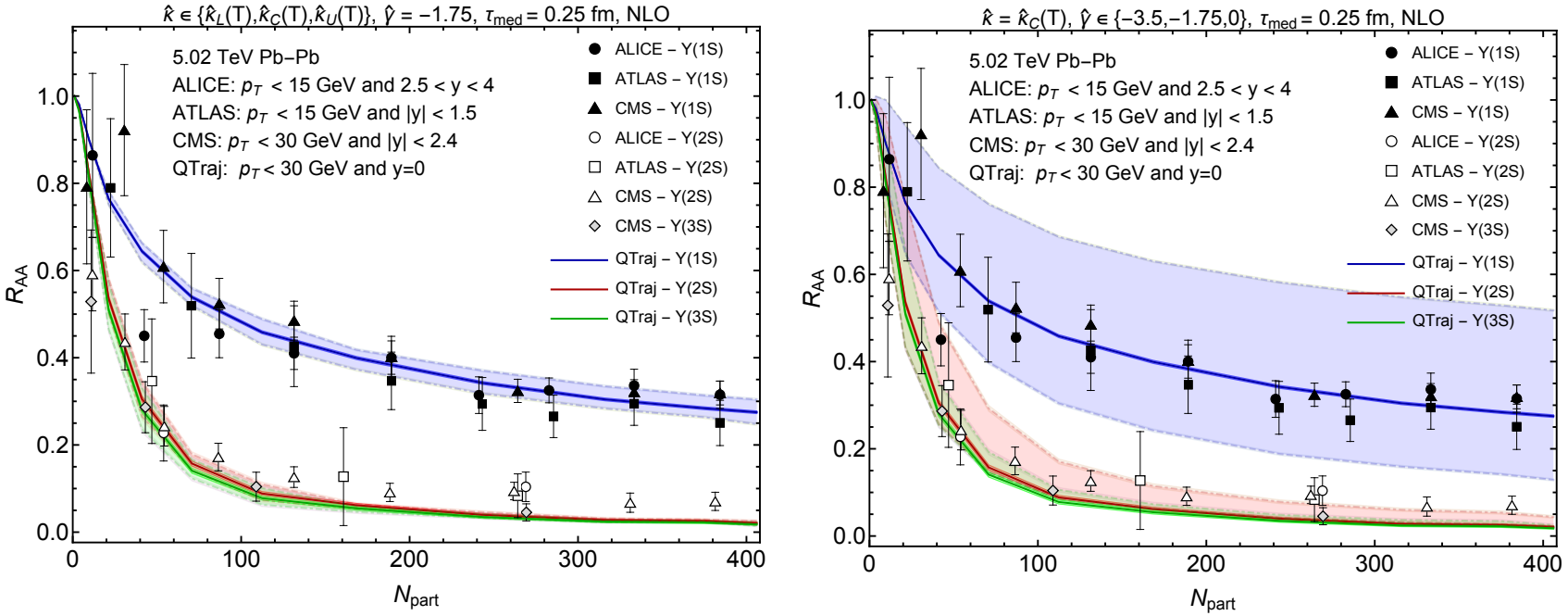

- Note that It is possible to use a shorter medium initialization time and obtain a similar description of the data.
- Above shows results using τ_{med} = 0.25 fm rather than 0.6 fm
- In this case, I changed the central value of gamma plotted, but the range of variation is the same.

Momentum-space anisotropies

4d flow tomography

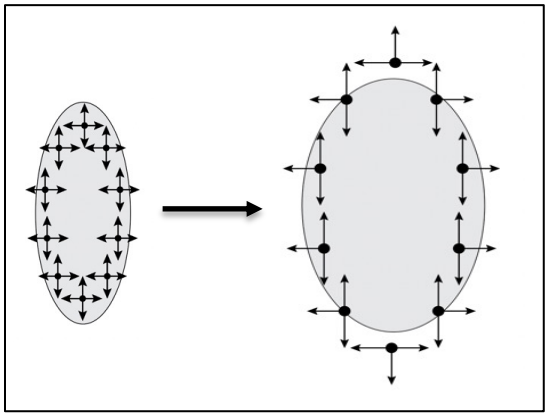

- Bottomonium probably doesn't flow in the "collective flow" sense.
- However, there can be momentum-space anisotropies induced by path-length differences in suppression along the short and long sides of the QGP.

Cern Courier, Fall 2019

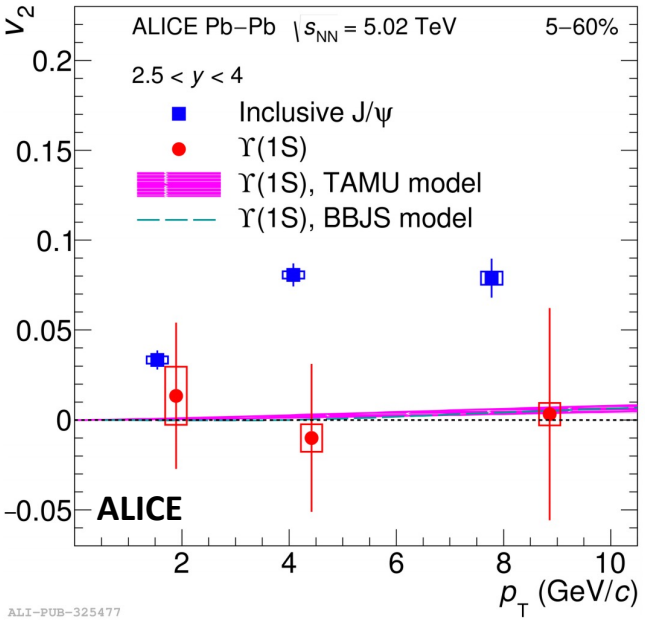

TAMU: Phys. Rev. C 96, (2017) 054901
BBJS: arXiv:1809.06235

ALICE Collaboration: arXiv:1907.03169

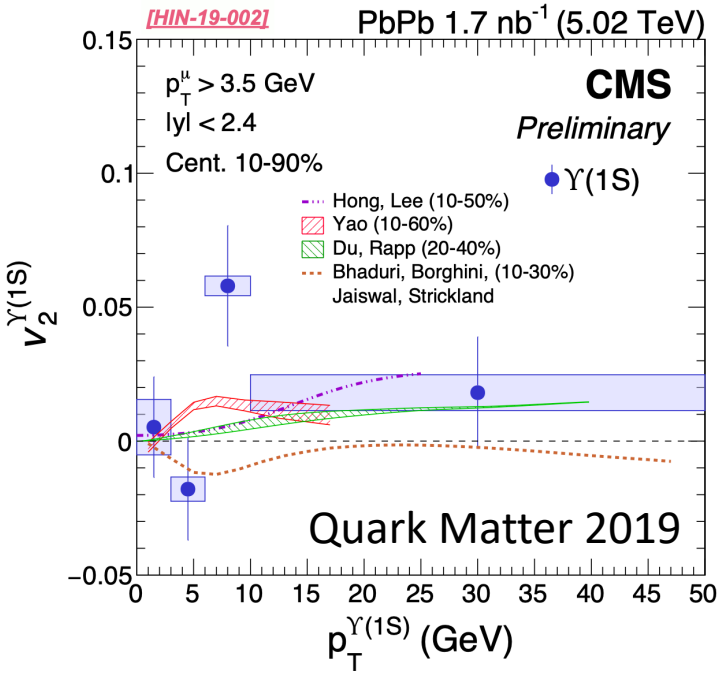

LO Momentum-space anisotropies at LHC

N. Brambilla, M.-A. Escobedo, M.S., A. Vairo, P. Vander Griend, and J.H. Weber, 2107.06222 (Leading-Order)

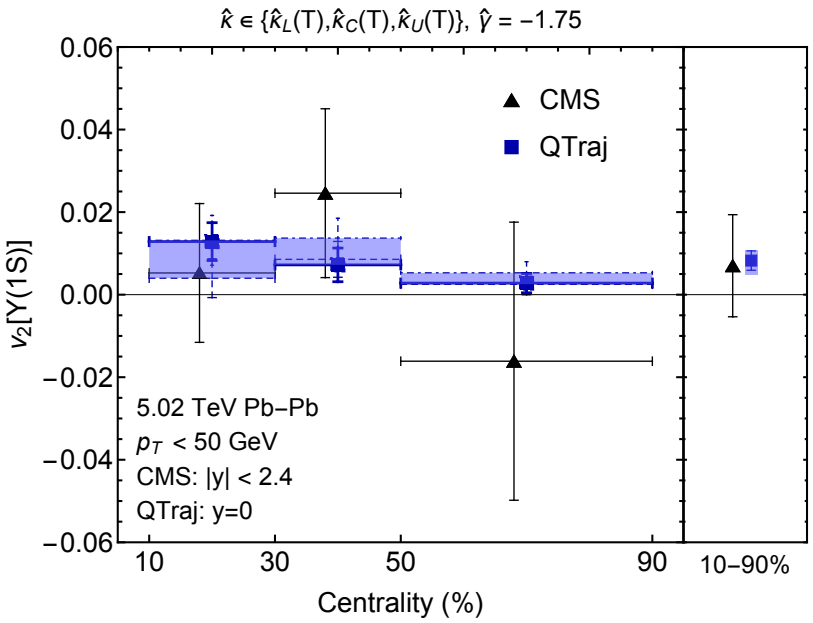

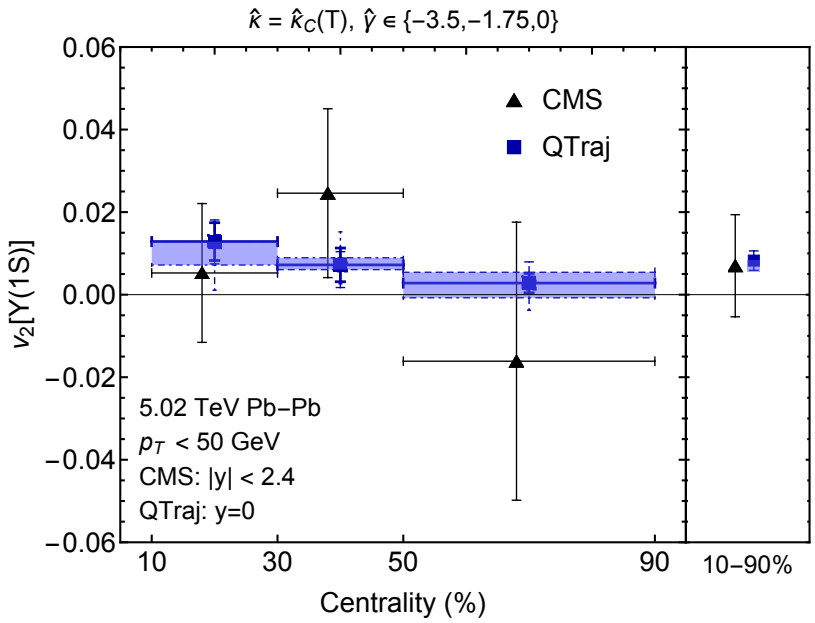

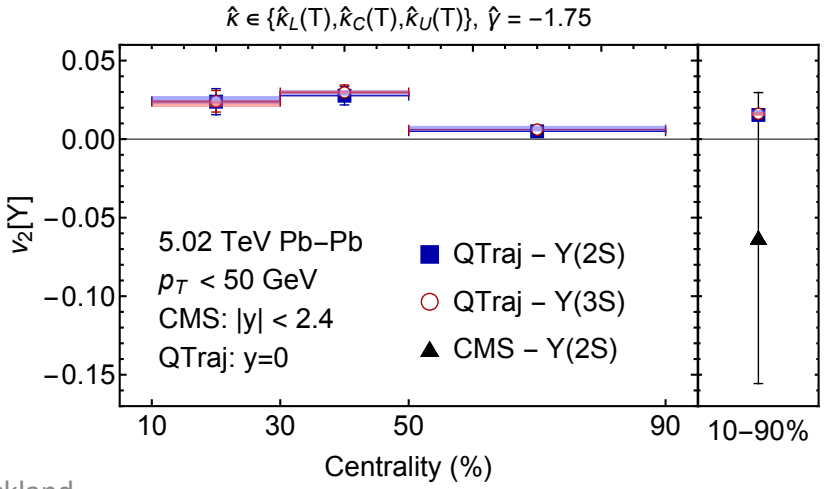

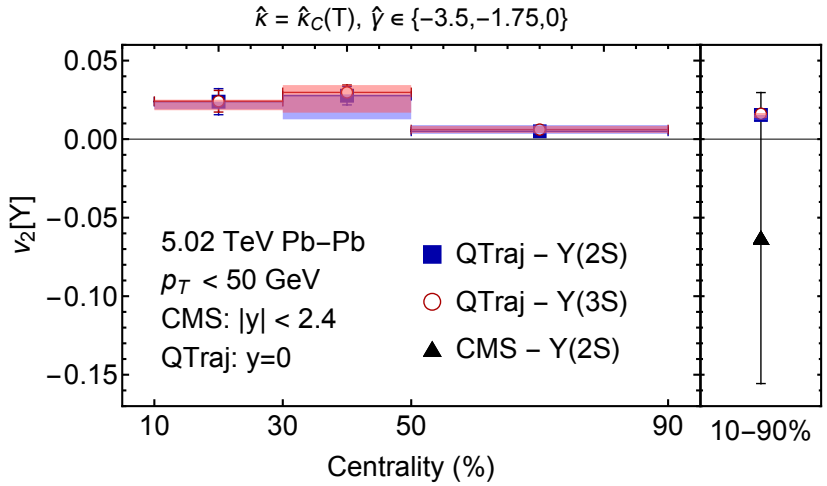

NLO Momentum-space anisotropies at LHC

H. Alalawi, J. Boyd, and M. Strickland, forthcoming

- Forthcoming work on including the effect of fluctuating hydrodynamics.
- Using MUSIC + IPGlasma IC tuned to 5.02 TeV Pb-Pb collisions.
- Agrees well with aHydro results for R_{AA} (not shown).

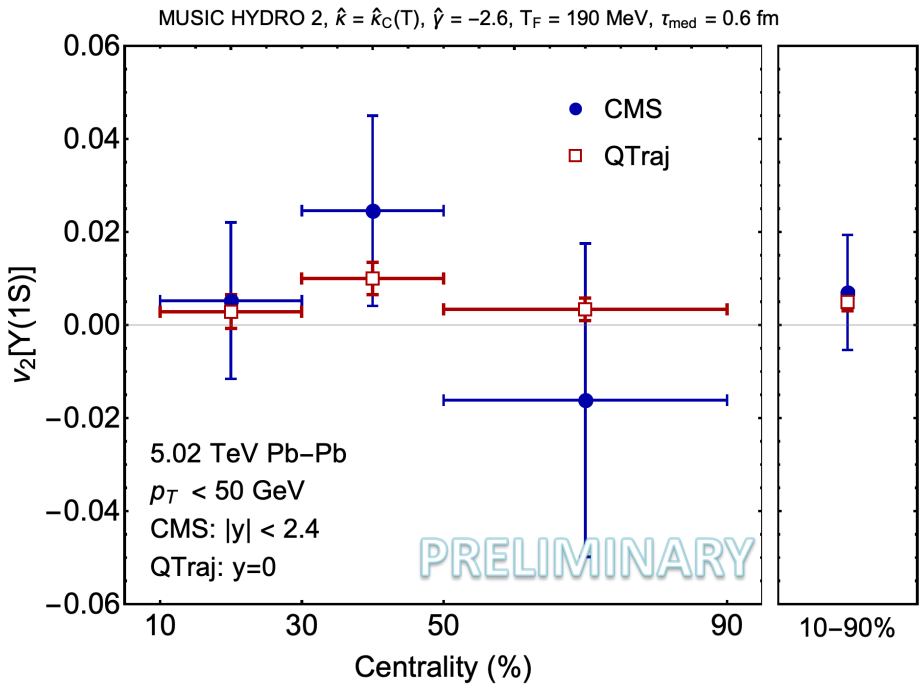

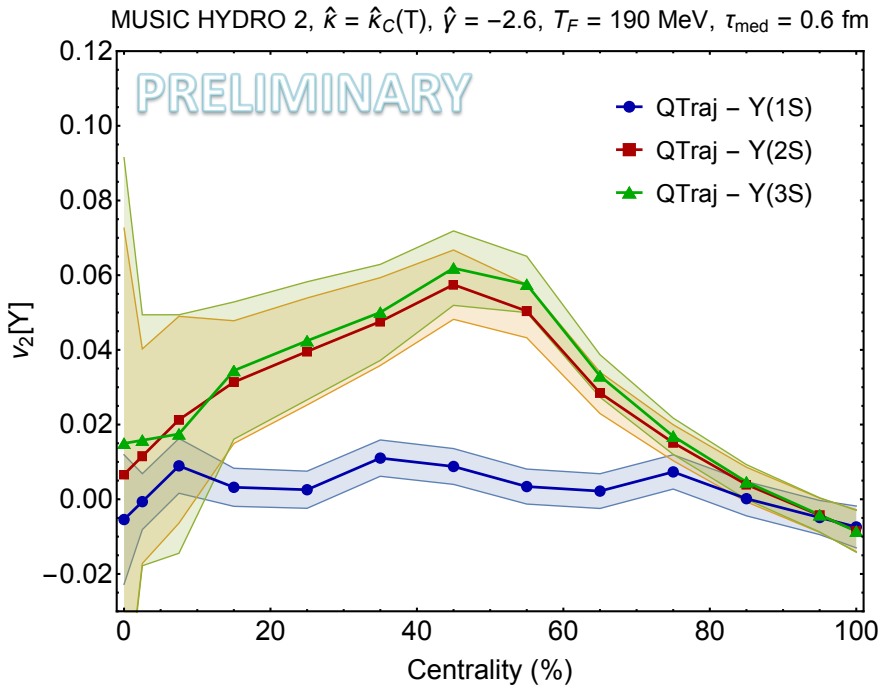

NLO OQS + pNRQCD predictions for R_{AA} vs N_{part} at RHIC

M. Strickland and S. Thapa, forthcoming

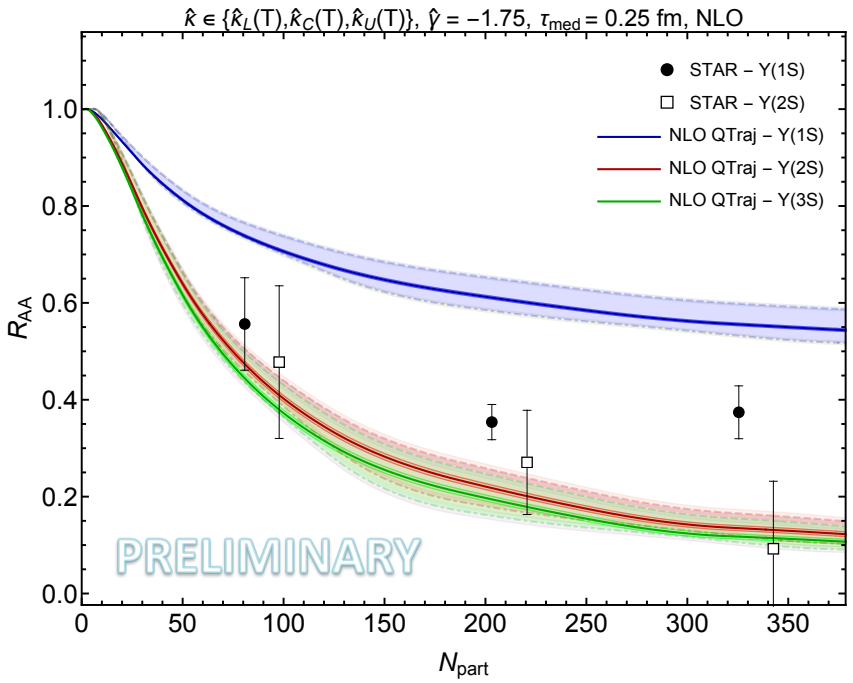

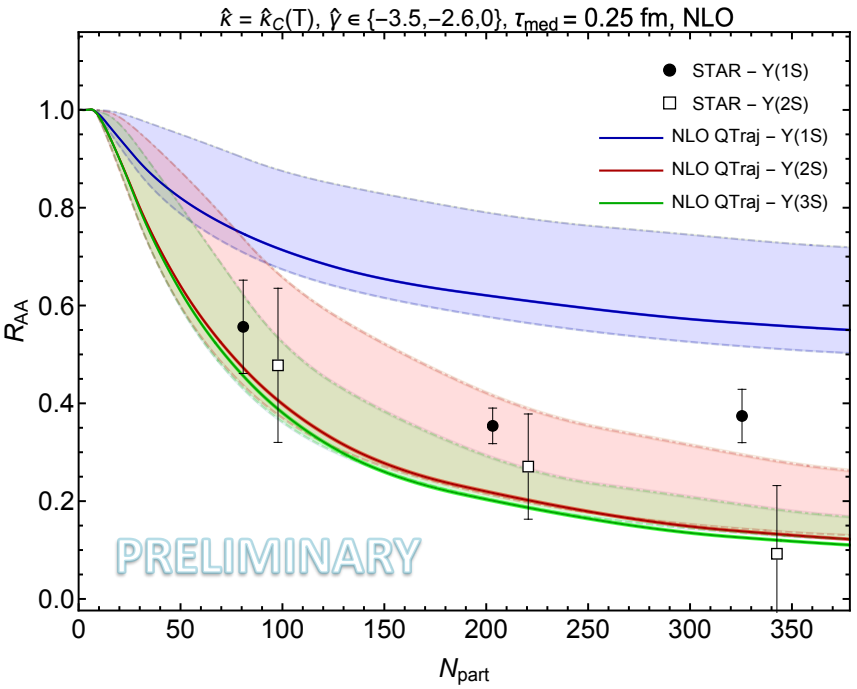

- Above are results from the NLO OQS + pNRQCD predictions for R_{AA} at 200 GeV compared to recently reported STAR data (2207.06568). Same parameters at LHC, only changed the hydrodynamic background.
- Framework does not predict enough 1S suppression
- STAR data indicate similar levels of suppression for the 1S and 2S for $N_{part} < 200$.
- Data from sPHENIX will be useful

Phenomenological KSU model RHIC predictions

A. Islam and M. Strickland, 2010.05457 and 2007.10211

M. Strickland and S. Thapa, forthcoming

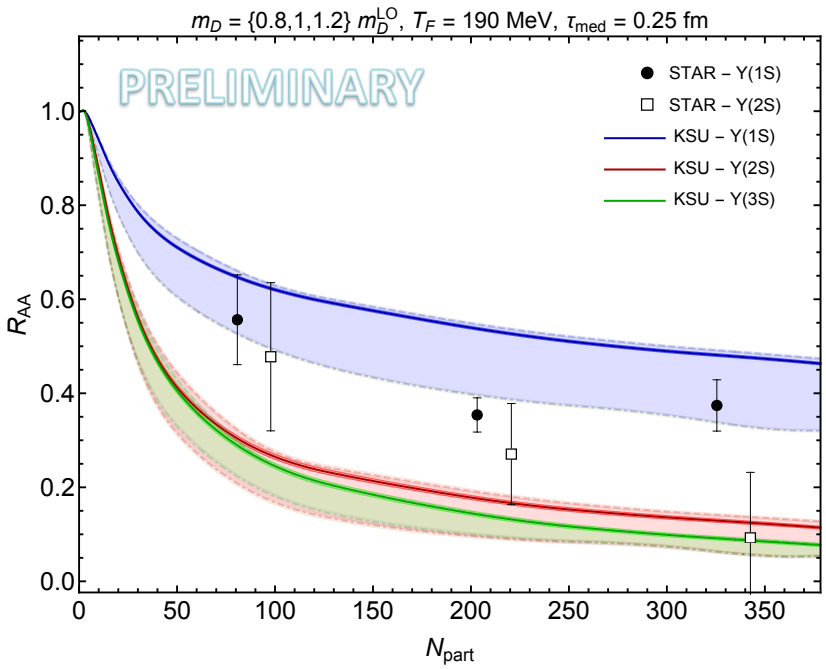

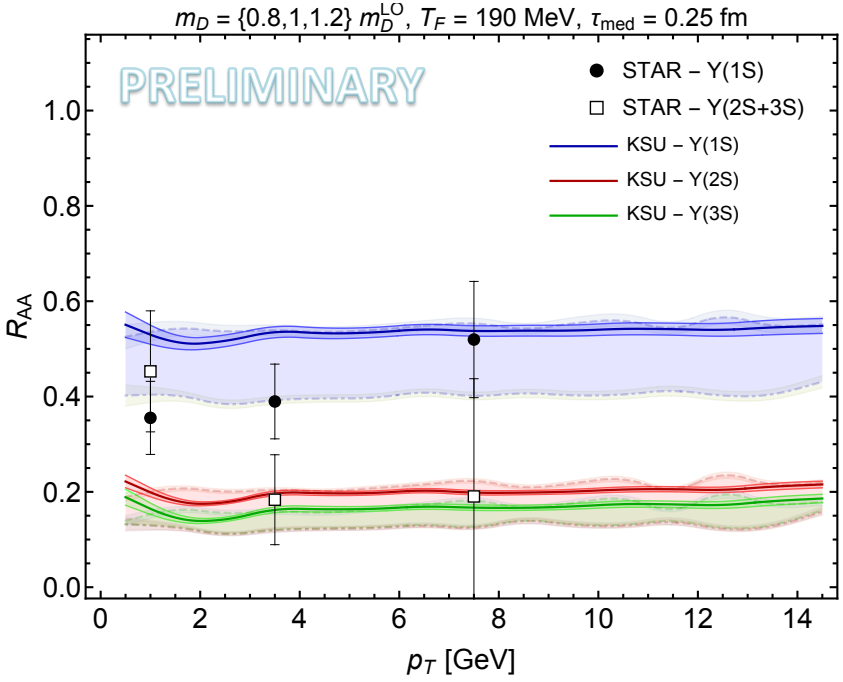

- Above are results from the KSU phenomenological potential.
- It reduces to a Cornell potential with string breaking at T=0. Parameterization gives all observed bottomium vacuum eigenenergies to a few %. For in-medium potential a KMS type potential is used for the real part and the Laine et al result for the imaginary part is used.
- The KSU model gets closer to the STAR data for the 1S, however, it can't explain the 2S results at the same time for $N_{part} < 225$. The transverse momentum dependence which is dominated by large N_{part} events, is reasonably well described.

Conclusions and Outlook

- **First 3D quantum non-abelian treatment of heavy quarkonium within the OQS+pNRQCD framework. Treatment has been extended to NLO in E/T.**
- Transport coefficients used were **constrained by independent lattice measurements.**
- **OQS + pNRQCD works quite well in describing bottomonium suppression and "flow" vs N_{part} and p_T seen at LHC energies.**
- However, the same setup, our preliminary results indicate that OQS + pNRQCD overpredicts R_{AA}[1S] at 200 GeV when compared with recent STAR data.
- Our preliminary results indicate that the phenomenological KSU model does better in describing R_{AA}[1S], however, it then underpredicts R_{AA}[2S].

Additional slides

Heuristic understanding – Noisy QM

- Heavy quark bound states have an in-medium potential with both real and imaginary parts. This is related to the large in-medium width.
- How can we understand the emergence of the imaginary part in a simple manner before leaping into open quantum systems + pNRQCD?
- **Consider a non-relativistic bound state subject to a noisy potential**

$$H(\mathbf{r},t) = -\frac{\nabla_{\mathbf{r}}^2}{M} + V(\mathbf{r}) + \Theta(\mathbf{r},t) \qquad \Theta(\mathbf{r},t) = \theta\left(\mathbf{R}+\frac{\mathbf{r}}{2},t\right) - \theta\left(\mathbf{R}-\frac{\mathbf{r}}{2},t\right)$$

Noise due to environment (assumed here to be color neutral).

- Noise has zero mean, is uncorrelated in time, and has a spatial correlation function $D(\boldsymbol{r})$

$$\langle\theta(\mathbf{x},t)\rangle = 0 \qquad \langle\theta(\mathbf{x},t)\theta(\mathbf{x}',t')\rangle = D(\mathbf{x}-\mathbf{x}')\delta(t-t')$$

Note: The treatment presented here does not include possibility of color-charged noise, more on this coming…

Heuristic understanding – Noisy QM

- Expanding the time evolution operator up to $O(\Delta t^{3/2})$

$$e^{-i\Delta t\, H(\mathbf{r},t)} \simeq 1 - i\Delta t\, H(\mathbf{r},t) - \frac{1}{2}\left\{\Delta t\, H(\mathbf{r},t)\right\}^2 + \ldots$$

$$\approx 1 - i\Delta t\left[H(\mathbf{r},t) - \frac{i}{2}\Delta t\left\{\theta(\mathbf{x},t)^2 + \theta(\mathbf{x}',t)^2 - 2\,\theta(\mathbf{x},t)\theta(\mathbf{x}',t)\right\}\right]$$

- Now construct an effective Hamiltonian that is averaged over the noise

$$\langle \mathrm{H}_{\mathrm{eff}}(\mathbf{r},t)\rangle \simeq H(\mathbf{r},t) - \frac{i}{2}\Delta t\left\{\langle\theta(\mathbf{x},t)^2\rangle + \langle\theta(\mathbf{x}',t)^2\rangle - 2\,\langle\theta(\mathbf{x},t)\theta(\mathbf{x}',t)\rangle\right\}$$

Imaginary part of the potential

$$\langle \mathrm{H}_{\mathrm{eff}}(\mathbf{r},t)\rangle = -\frac{\nabla^2_{\mathbf{r}}}{M} + V(\mathbf{r}) - i\left\{D(\mathbf{0}) - D(\mathbf{r})\right\}$$

$$\Im[V(r)] = D(\mathbf{r}) - D(\mathbf{0})$$

Imaginary part emerges through interference of wave function with itself when summing over environmental noise.

A parallelizable approach: Quantum trajectories

N. Brambilla, M.-A. Escobedo, M.S., A. Vairo, P. Vander Griend, and J.H. Weber, 2012.01240

$$\frac{d\rho_{\rm probe}}{dt} = -iH_{\rm eff}\rho_{\rm probe} + i\rho_{\rm probe}H_{\rm eff}^{\dagger} + \sum_n C_n\,\rho_{\rm probe}\,C_n^{\dagger}$$

Non-unitary "no jump" evolution

Can treat this "quantum jump" term stochastically

- Can be reduced to the solution of a large set of "quantum trajectories" in which we solve a 1D Schrödinger equation with a **non-Hermitian Hamiltonian $H_{\rm eff}$,** subject to **stochastic quantum jumps**.
- The evolution with the non-Hermitian $H_{\rm eff}$ preserves the color and angular momentum state of the system (but not norm).
- Collapse/jump operators encode transitions between different color/angular momentum states (subject to selection rules).

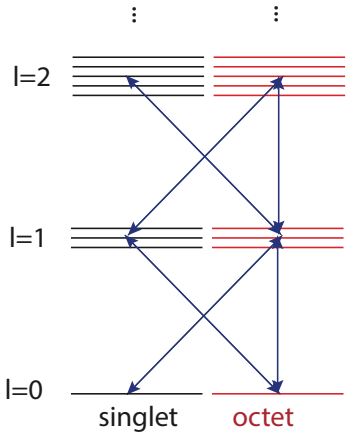

- For each **physical trajectory** (path through the QGP) we average over a large set of **independent quantum trajectories** → **Embarrassingly parallel**
- **Added benefit: Can describe all angular momentum states (no cutoff) .**

How can one numerically solve these equations?

$$\frac{d\rho_{\rm probe}}{dt} = -iH_{\rm eff}\rho_{\rm probe} + i\rho_{\rm probe}H_{\rm eff}^{\dagger} + \sum_n C_n\,\rho_{\rm probe}\,C_n^{\dagger}$$

- Each block of the density matrix in color space can be decomposed into orbital angular momentum blockwise.
- Upon truncating in angular momentum ($l \leq l_{max}$) one can reduce both the singlet and octet blocks of the reduced density matrix to size $(l_{max}+1)^2$.
- One can then discretize the radial wavefunction (N = # of lattice points) and evolve the reduced density matrix using standard differential equation and matrix solvers gives $\sim N^2(l_{max}+1)^2$ matrix size.
- **Need to describe bound and unbound states with highly localized initial wave function, so the box must be large and have small lattice spacing → large N and large l_{max}.**
- As N and l_{max} become large, **the computation becomes very challenging**.
- **Need a better/faster method which we can easily parallelize.**

Initial bottomonium wavefunction

- We took the initial wavefunction to be given by a smeared delta function (local production due to large mass, Δ ~ 1/M) of the form

$$u_\ell(r, \tau = 0) \propto r^{\ell+1} \exp(-r^2/\Delta^2)$$

- For a given l, the **initial state is a quantum linear superposition** of the eigenstates of H.
- **Includes both bound and unbound states.**
- We took $\Delta = 0.2\ a_0$ which reproduces results obtained with a true delta to within 1%.

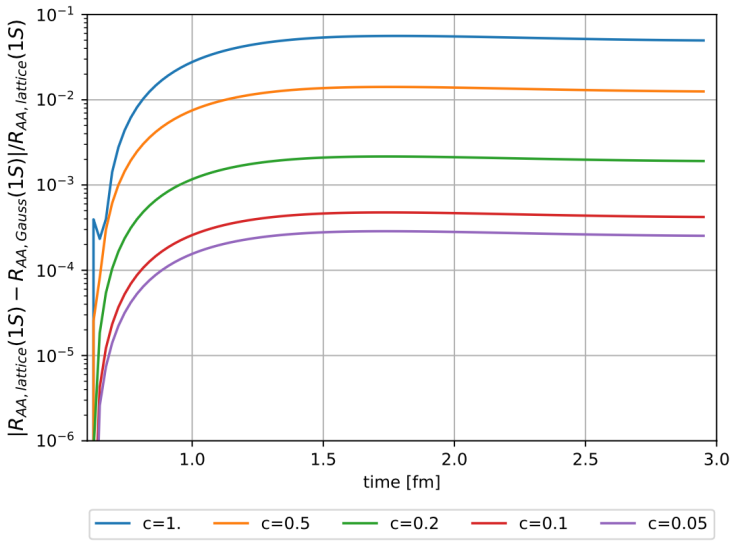

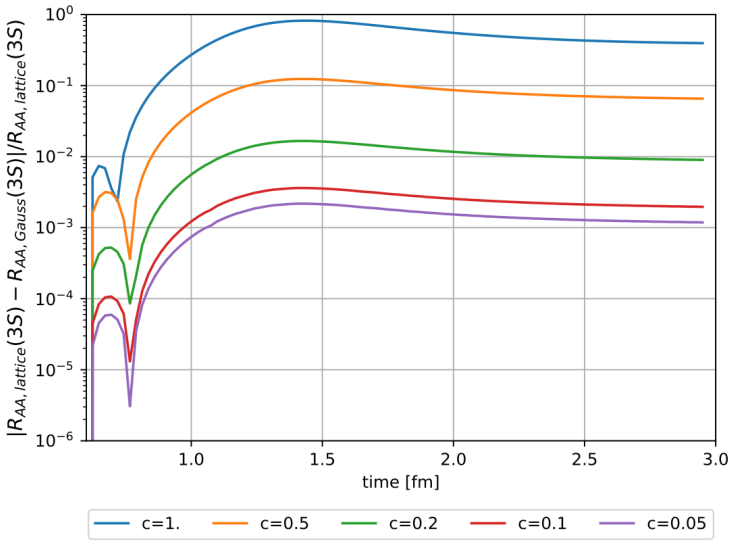

3+1D hydrodynamical background

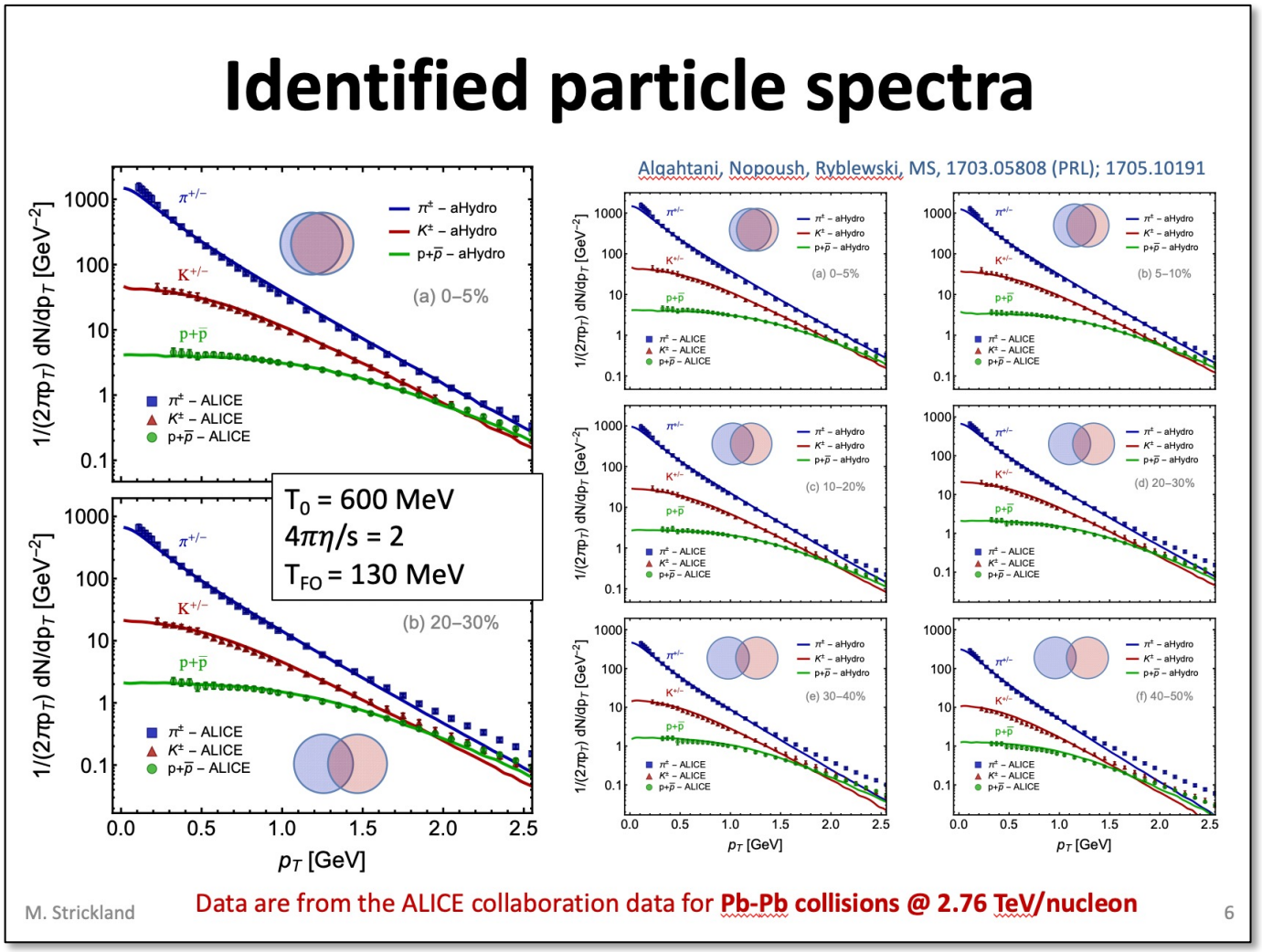

- We use a 3+1D dissipative code for the hydro background (quasiparticle anisotropic hydrodynamics)
- Has been tuned to RHIC and LHC heavy ion collisions
- Reproduces spectra, multiplicities, identified elliptic flow of light hadrons, HBT radii, etc.

For 5.02 TeV, T_0 = 630 MeV @ t_0 = 0.25 fm/c